crystals

MDPI

Article

Evaluation of Growth, Thermal, and Spectroscopic Properties of Er^{3+}-Doped CLNGG Crystals for Use in 2.7 μm Laser

Kaiyang Tang [1,2], Shawuti Yingming [2,3], Jinggang Gai [1,*] and Zhongben Pan [2,*]

1 State Key Laboratory of Polymer Materials Engineering, Polymer Research Institute of Sichuan University, Chengdu 610065, China; tangkaiyang@stu.scu.edu.cn
2 Institute of Chemical Materials, China Academy of Engineering Physics, Mianyang 621900, China; savut@stu.xju.edu.cn
3 School of Physics and Technology, Xinjiang University, Urumqi 830046, China
* Correspondence: gaijinggang@scu.edu.cn (J.G.); zhongbenpan@caep.cn (Z.P.)

Abstract: A series of optical-quality Er^{3+}-doped calcium lithium niobium gallium garnet (CLNGG) single crystals with different Er^{3+} ion concentration (10, 15 and 30 at.%) has been grown by the Czochralski method. A comparative study of their structure, thermal, and spectroscopic properties is performed. Crystal structure was analyzed with X-ray powder diffraction (XRPD) and refined by the Rietveld method, results showing that the Er:CLNGG crystal possesses a cubic structure with space group $Ia\bar{3}d$, and the lattice constants decrease linearly as the Er^{3+} concentration increase. The complete set of thermal properties were systematically studied for the first time. It has been found that all the thermal conductivities increase with temperature, indicating a glass-like behavior. Effect of Er^{3+} concentration on spectroscopic properties of Er:CLNGG crystals was studied. Results show that with the Er^{3+} concentration increase, the NIR fluorescence around 1600 nm weakens, while the Mid-IR fluorescence intensity around 2700 nm strengthens. Fluorescence lifetime of $^4I_{13/2}$ decreased faster than that of $^4I_{11/2}$ with the Er^{3+} concentration increase, which is beneficial for surmounting the "bottleneck" effect to achieve 2.7 μm laser. All the results show that CLNGG crystal with high Er^{3+} concentration is a potential candidate for the 2.7 μm laser.

Keywords: Er:CLNGG crystal; thermal properties; spectroscopic properties; 2.7 μm laser

Citation: Tang, K.; Yingming, S.; Gai, J.; Pan, Z. Evaluation of Growth, Thermal, and Spectroscopic Properties of Er^{3+}-Doped CLNGG Crystals for Use in 2.7 μm Laser. *Crystals* **2021**, *11*, 126. https://doi.org/10.3390/cryst11020126

Academic Editor: Chiashain Chuang
Received: 5 January 2021
Accepted: 24 January 2021
Published: 27 January 2021

1. Introduction

Mid-infrared (MIR) laser sources in the 2.7 μm spectral range activated by Er^{3+} ions ($^4I_{11/2}\rightarrow{}^4I_{13/2}$) are under rapid development nowadays due to their potential in various applications, e.g., medical technology, environmental protection and detection due to the strong absorption by water [1,2]. Besides, lasers in this region are also an ideal pump source for 3–15 μm optical parametric oscillation (OPO) lasers [3,4].

By far, various Er^{3+}-doped gain materials had been reported, such as the garnet (crystals and ceramics) YAG [5], GGG [6], LuGG [7], YGG [8], YSGG [9–12], GSGG [13,14], the sesquioxide (crystals and ceramics) Y_2O_3 [15,16], Lu_2O_3 [17], and the fluoride (crystals, ceramics, and fibers) CaF_2 [18,19], SrF_2 [20], $LiYF_4$ [21], ZBLAN [22]. However, the fluorescence lifetime of the upper laser level $^4I_{11/2}$ is much shorter than that of the lower laser level $^4I_{13/2}$, which is considered to be self-terminating, making the population inversion difficult and impeding laser oscillations. Generally, to overcome such self-terminating bottleneck effect, codoping of proper ions, such as Pr^{3+} or Tm^{3+}, can effectively shorten the fluorescence lifetime of the lower laser level $^4I_{13/2}$ owing to the energy transfer between electrons on $^4I_{11/2}$ and $^4I_{13/2}$ states [1,23]. Doping with high Er^{3+} concentration is another effective option, which can promote the energy transition among active ions for reducing the fluorescence lifetime of the lower laser level $^4I_{13/2}$ and suppress the self-terminating effect.

In this work, we selected disordered calcium lithium niobium gallium garnet (shortly CLNGG) as the host matrix, which belongs to the cubic crystal class (sp. gr. $Ia\bar{3}d$). Com-

pared with the conventional ordered garnet crystal, such as YAG, CLNGG has at least two advantages due to its excellent physical and chemical characteristics. Firstly, the much lower melt point (~1450 °C) makes it easy to obtain high quality and large-sized crystal by using the conventional Czochralski (Cz) method. Besides, due to a random distribution of the Ga^{3+} and Nb^{5+} cations over the same lattice sites (octahedral and tetrahedral), it has a disordered structure, which can lead to splitting and inhomogeneous broadening of the spectral bands of the Re^{3+} dopants, making it very suitable for ultra-short pulse generation [24]. However, to our knowledge, there is almost no report about the Er^{3+}-doped CLNGG. Thus, a series of optical-quality Er^{3+}-doped CLNGG single crystals was grown by the Cz method. A comparative study of their structure, thermal, and spectroscopic properties is performed to evaluate its application in 2.7 μm laser.

2. Experimental Section

2.1. Crystal Growth

A series of Er:CLNGG crystals was grown by the conventional Cz method. High-purity $CaCO_3$ (purity: 4N), Nb_2O_5 (4N), Ga_2O_3 (5N), Er_2O_3 (5N) and Li_2CO_3 (5N) powder were used and exactly weighed. For the preparation of polycrystalline Er:CLNGG, a certain amount of Er_2O_3 with Er^{3+} concentration equal to 10, 15, and 30 at.% was introduced according to the following solid-state reaction:

$$\frac{x}{3}CaCO_3 + \frac{0.275x}{2}Li_2CO_3 + \frac{1.775x}{2}Nb_2O_5 + \frac{5-2.95x}{2}Ga_2O_3 + \frac{3(1-x)}{2}Er_2O_3$$

$$\rightarrow (Ca_3Li_{0.275}Nb_{1.775}Ga_{2.95}O_{12})_x(Er_3Ga_5O_{12})_{1-x} + \frac{2.825x}{6}CO_2$$

In order to compensate the volatilization of Ga_2O_3, during the experiment, an excess of 1.5 wt.% Ga_2O_3 was added. Besides, to further avoid the volatilization of Ga_2O_3 and Li_2O, the crystals were grown under 10% CO_2 + 90% Ar atmosphere. The raw materials were mixed for 24 h and heated at 920 °C for 10 h in a platinum crucible to decompose $CaCO_3$. When the materials were cooled down to room temperature (293.15 K), the mixture was again grounded, mixed, and pressed into tablets under high pressure. Then the materials were sintered at 1200 °C for 20 h to synthesis polycrystalline materials. The polycrystalline materials were heated by an intermediate-frequency heater. An oriented CLNGG seed with [111] direction was used for crystal growth. During the crystal growth, the puling rate and rotation speed were 0.6–2 mm/h and 11 rpm, respectively. When crystal growth process was completed, the single crystal was cooled down to room temperature at the speed of 10–20 °C/h.

The photograph of crystal was shown in Figure 1a–f, it was clear that the as-grown crystals have almost no macroscopic defects. The as-grown crystals were pink owing to the introduction of Er^{3+} ions and annealing would make crystal more transparent. It was worth noting that the 15 at.% Er:CLNGG crystal was darker than other crystals, which might attribute to uncertain atmosphere and evaporation of Ga_2O_3 during the experiment.

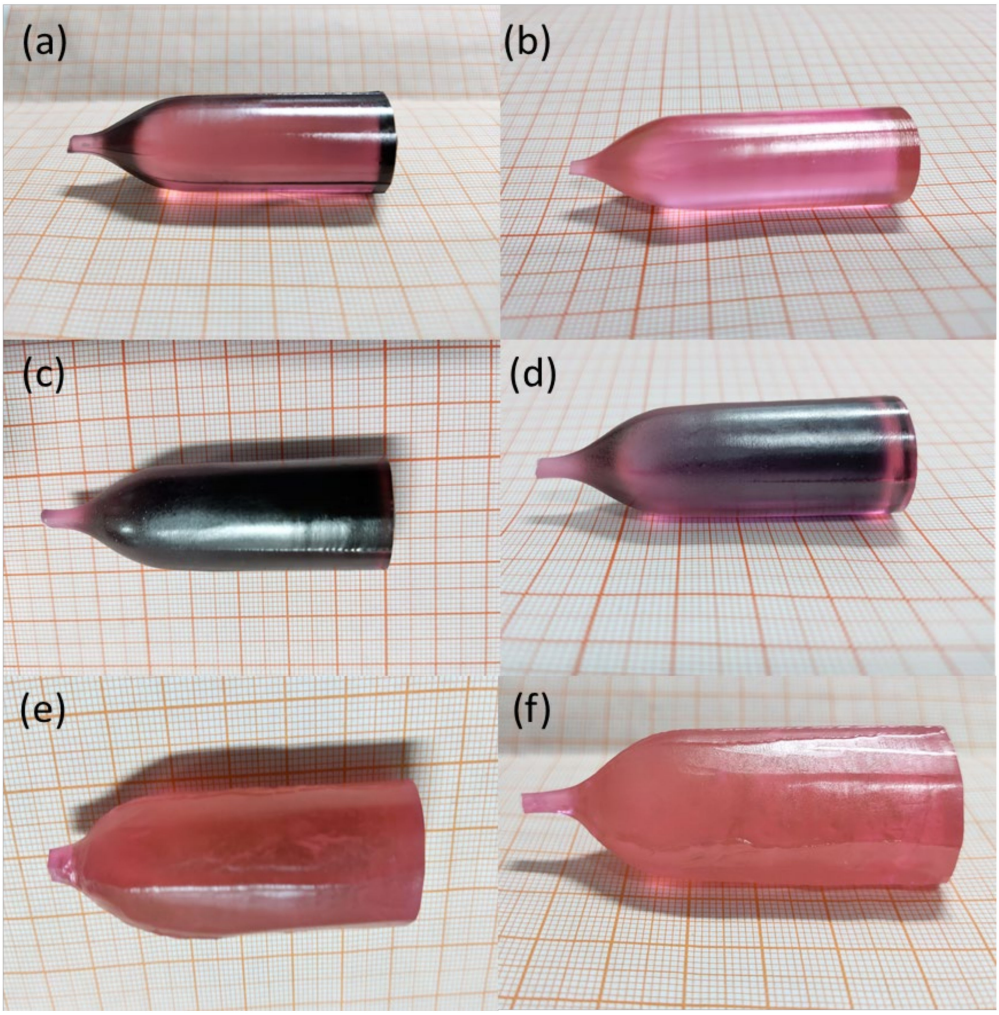

Figure 1. Images of crystal for (**a**) 10 at.% Er:CLNGG before annealing (**b**) 10 at.% Er:CLNGG after annealing (**c**) 15 at.% Er:CLNGG before annealing (**d**) 15 at.% Er:CLNGG after annealing (**e**) 30 at.% Er:CLNGG before annealing (**f**) 30 at.% Er:CLNGG after annealing.

2.2. Measurement

The structure and crystallographic data of Er:CLNGG crystal was studied by X-ray powder diffraction (Bruker D2 Phaser diffractometer, Karlsruhe, Germany) with Cu-Kα1 radiation (λ = 1.5418 Å). The XRD pattern was measured in the 2θ range from 10 to 90° with a step size of $0.02^{\circ}\cdot s^{-1}$.

Effective segregation coefficient of Er^{3+} ions was confirmed by inductively coupled plasma-optical emission spectroscopy (ICP-OES). Effective segregation coefficient K_{eff} can be calculated by the following equation:

$$k_{eff} = \frac{C_s}{C_l} \quad (1)$$

In the equation, C_s and C_l were the concentrations of Er^{3+} in the crystal and melt, respectively. The C_l of raw material was 10 at.%, 15 at.%, and 30 at.%, while the concentrations of Er^{3+} in the crystal were measured to be 14.72 at.%, 23.68 at.%, and 41.36 at.%, respectively. Thus the k_{eff} of the Er^{3+} in the as-grown crystal was 1.472, 1.579 and 1.378 for 10 at.%, 15 at.%, and 30 at.%, respectively. Furthermore, by using the calculated unit-cell parameters and the

following equation, the Er^{3+} ion concentration N_{Er} for the as-grown crystals can be determined to be 1.92×10^{21}, 2.29×10^{21}, and 6.21×10^{21} ions/cm^3, respectively.

$$N_{Er} = \frac{Z \times C_l \times K_{eff}}{a \times b \times c} \quad (2)$$

Here a, b, and c are the unit-cell parameters, Z is the number of the formula units.

The specific heat was studied by simultaneous thermal analyzer (Perkin Elmer Diamond: DSC, Waltham, MA, USA). The thermal diffusivity coefficient was measured by the laser flash method using a laser flash apparatus (NETZSCH LFA457, Selb, Germany). The sample used for the measurement was made into crystal plate with the dimensions of $4 \times 4 \times 1$ mm^3, and both sides of each sample were coated with graphite.

For the spectroscopic study, all the samples were cut to the cube with the dimensions of $3 \times 3 \times 3$ mm^3 and the 3×3 mm^2 faces that perpendicular to [111] direction were polished. The absorption spectra were recorded by UH4150 spectrophotometer (Direct Light Detector, Hitachi, Ltd, Tokyo, Japan) at room temperature. The scan speed was 120 mm/min and the sampling interval was 1.00 nm. The emission spectra and fluorescence lifetimes were measured by an Edinburgh Instruments spectrophotometer (FSP920c, Livingston, UK), under 987 nm pumping with a 5 ns pulse of an optical parametric oscillator. The ratio of signal to noise (SNR) is about 6000:1 and the resolution ratio of this equipment for the measurement of emission spectra is less than 0.05 nm, while for the measurement of fluorescence lifetimes, the minimum time resolution is less than 610 fs.

3. Results and Discussion

3.1. Structure Refinement

For the confirmation of the composition and phase purity of the as-grown 10, 15, and 30 at.% Er:CLNGG crystals, Figure 2a displays the XRD patterns of the Er:CLNGG samples. All the diffraction peaks are well indexed with the garnet calcium tin silicon gallium oxide (PDF card #96-100-1563) having a cubic structure. The diffraction peaks corresponding to any other impurities were not observed which verifies the successful incorporation of Er^{3+} ions into the host structure without significant lattice distortion.

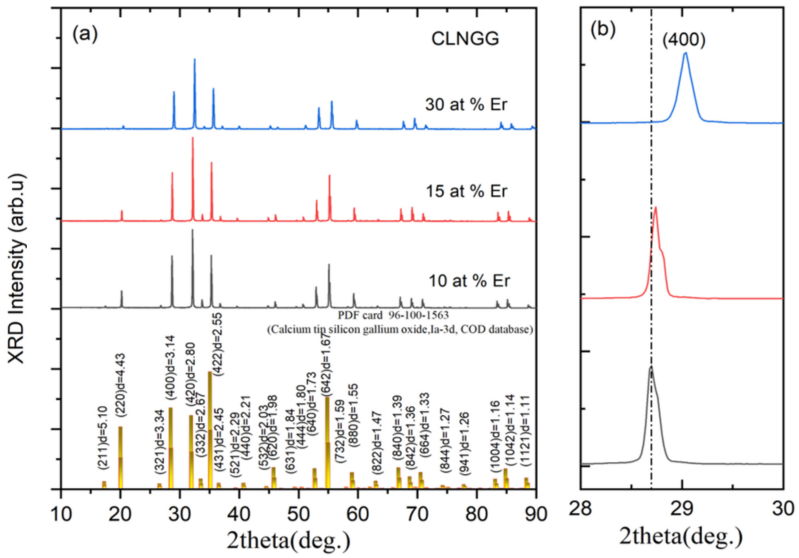

Figure 2. (**a**) Room-temperature X-ray powder diffraction (XRD) pattern of Er:CLNGG crystal and the reference pattern of calcium tin silicon gallium oxide: garnet phase with $Ia\bar{3}d$ space group (PDF card #96-210-1676) (**b**) the magnified XRD patterns with the selected diffraction peaks from 28 to 29° for 10, 15 and 30 at.% Er:CLNGG crystals.

According to the effective ionic radii of cations with the corresponding coordination number (CN), we suggest that the activator Er^{3+} is expected to occupy the Ca^{2+} sites randomly in the CLNGG host, because the effective ionic radii of Er^{3+} (Ri = 1.004 Å for CN = 8) is closest to that of Ca^{2+} (Ri = 1.120 Å for CN = 8) [25]. The substitution of Ca^{2+} by Er^{3+} will have a change in the lattice parameters. Indeed, the representative diffraction peak of 10, 15, and 30 at.% Er:CLNGG appeared in the diffraction angle range from 28 to 30° is shown in Figure 2a. Clearly, the characteristic peak (400) shifts gradually to higher angles with the Er^{3+} content increase. Thus, with referring to the relation between the interplanar spacing d_{hkl} and the parameter "a" (2), this behavior derived from the decrease of the lattice volume and to express it clearly, the lattice parameters were calculated and listed in Table 1, with the increase of Er^{3+} doping concentration, the cell dimension a is gradually decreased.

$$\frac{1}{d_{hkl}^2} = \frac{h^2 + k^2 + l^2}{a^2} \quad (3)$$

Table 1. Crystallographic data and refinement parameters for 10, 15 and 30 at.% Er:CLNGG.

Data	10 at.% Er:CLNGG	15 at.% Er:CLNGG	30 at.% Er:CLNGG
Crystal System		Cubic	
Space group		$Ia\bar{3}d$	
Laue Class		m-3m	
General multiplicity		96	
Calculated density (g/cm^3)	4.501	5.312	5.988
Lattice constant a (Å)	12.4929(2)	12.4767(8)	12.4485(8)
α (deg.)		90	
Volume ($Å^3$)	1949.808	1942.260	1929.120
2θ range (deg.)		10–90	
2θ step		0.02	
Radiations		Cu-Kα1 (λ = 1.5418 Å)	
No. of reflections	151	148	166
Refinement software		Match3! (crystal impact) software	
Reliability factors	Rp = 3.58, Rwp = 4.88, Rexp = 2.47 and χ^2 = 3.90	Rp = 3.40, Rwp = 4.65, Rexp = 2.59 and χ^2 =3.21	Rp = 2.85, Rwp = 3.89, Rexp = 2.38 and χ^2 = 2.68

To obtain the detailed structural information of Er:CLNGG crystals, the Rietveld refinement is implemented using the match3! software. Figure 3a–c exhibits the refined XRD profiles of 10, 15 and 30 at.% Er:CLNGG. The crystal data CNGG was adopted as an initial refinement model [26]. The refinement is utilized to determine the possible sites of constituents Ca | Er, Nb | Ga, and Nb | Ga | Li cations occupy the dodecahedron, octahedron, and tetrahedron sites, respectively. Detailed crystallographic data extracted from the refinement and fitting parameters, such as expected R factor (Rexp), weighted-profile R factor (Rwp), and goodness of fittings (GOF (χ) = Rwp/Rexp), are summarized in Table 1, and the refined structural parameters and atomic positions are summarized in Table 2. The value of χ^2 is smaller than 4 for the three different doping concentrations, indicating the reliable fitting of the experimental and computed data. The crystal structure of the Er:CLNGG crystals was identified as the cubic garnet with the centrosymmetric space group $Ia\bar{3}d$. The lattice parameter increased linearly with the incorporation of the Er^{3+}, which is described by the Vegard's law [27]. This finding suggested that the doped Er^{3+} ions were efficiently incorporated on the Ca^{2+} sites in the host lattice.

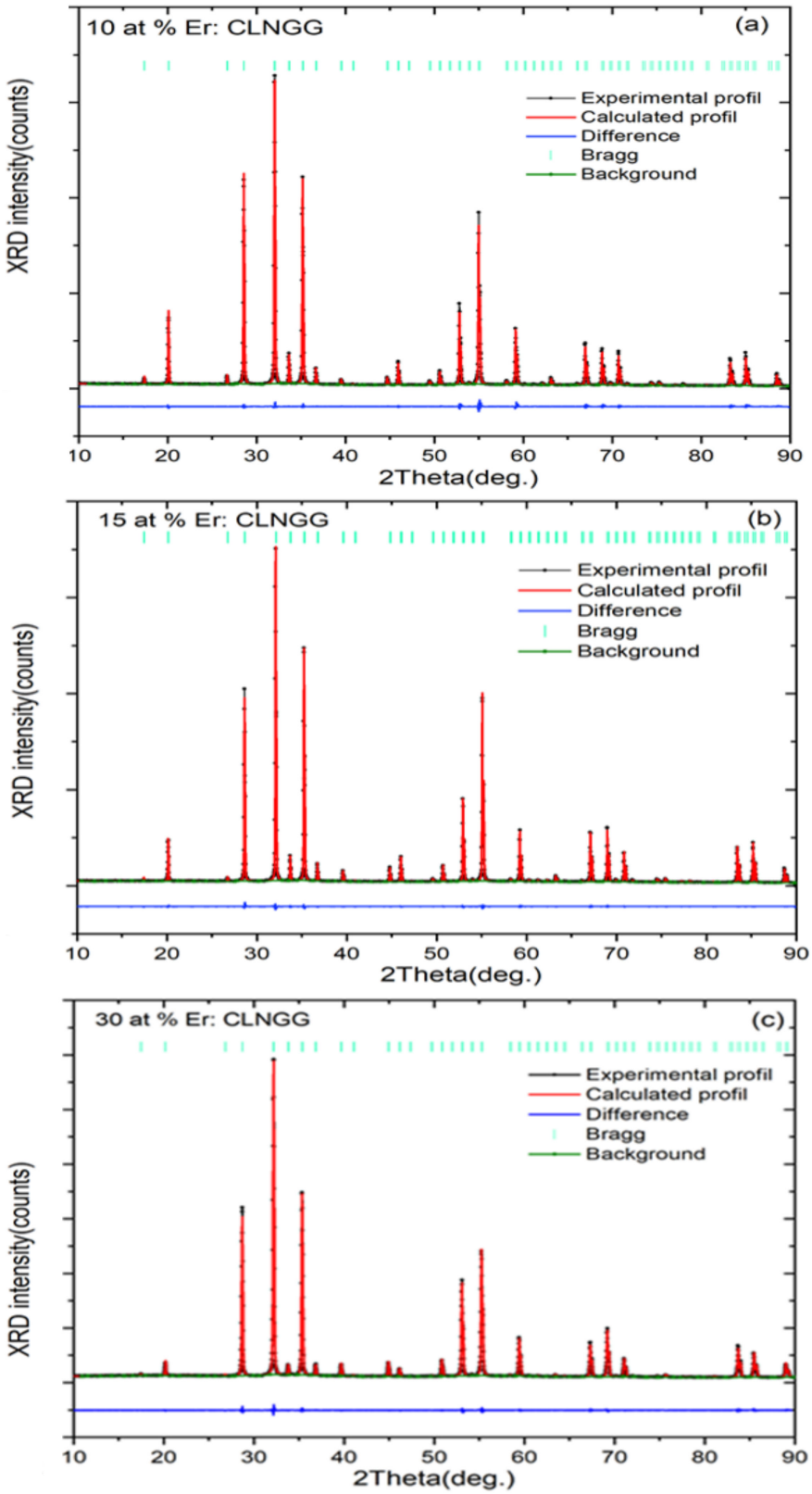

Figure 3. Rietveld structure refinement plots for: (**a**) 10 at.% Er: CLNGG (**b**) 15 at.% Er: CLNGG (**c**) 30 at.% Er: CLNGG.

Table 2. Atomic coordinates, sites, occupancy factors (O.F) and isotropic displacement parameters Biso (Å^2) for 10, 15, and 30 at.% Er:CLNGG crystals.

Atoms	Site	10 at.% Er:CLNGG				
		x/a	y/b	z/c	O.F	Biso(Å^2)
Ca | Er	24c	0.1250	0	1/4	0.9 | 0.1	0.925(1)
Nb1	16a	0	0	0	0.660	1.011(2)
Ga1	16a	0	0	0	0340	1.011(2)
Ga2	24d	0.3750	0	1/4	0.820	1.102(3)
Nb2	24d	0.3750	0	1/4	0.069	1.102(3)
Li	24d	0.3750	0	1/4	0.099	1.102(3)
O	96h	0.5393(7)	0.1507(5)	0.9754(4)	1	1.295(5)
Atoms	**Site**	**15 at.% Er:CLNGG**				
		x/a	y/b	z/c	O.F	Biso(Å^2)
Ca | Er	24c	0.1250	0	1/4	0.85 | 0.15	0.971(2)
Nb1	16a	0	0	0	0.66	1.092(1)
Ga1	16a	0	0	0	0.34	1.092(1)
Ga2	24d	0.3750	0	1/4	0.762	1.221(3)
Nb2	24d	0.3750	0	1/4	0.069	1.221(3)
Li	24d	0.3750	0	1/4	0.138	1.221(3)
O	96h	0.5461(6)	0.1516(5)	0.9672(5)	1	1.531(7)
Atoms	**Site**	**30 at.% Er:CLNGG**				
		x/a	y/b	z/c	O.F	Biso(Å^2)
Ca | Er	24c	0.1250	0	1/4	0.7 | 0.3	0.997(1)
Nb1	16a	0	0	0	0.660	1.056(1)
Ga1	16a	0	0	0	034	1.056(1)
Ga2	24d	0.3750	0	1/4	0.736	1.112(5)
Nb2	24d	0.3750	0	1/4	0.069	1.112(5)
Li	24d	0.3750	0	1/4	0.170	1.112(5)
O	96h	0.5573(5)	0.1565(4)	0.9602(7)	1	1.613(1)

Figure 4 shows the unit cell of the cubic structure, projected on the (110) crystallographic plan of Er:CLNGG oxide garnet, the structure had been generated from the computed atomic coordinates. CLNGG belongs to the family of cubic multicomponent garnets with a general formula $\{A\}_3[B]_2(C)_3O_{12}$, where {A} represented a cation in the dodecahedral (8-fold) site, which was represented by 24c as Wyckoff position. [B] and (C) represent cations in octahedral (6-fold) site (16a) and in the tetrahedral (4-fold) site (24d), respectively. All the oxygen anions occupy tetrahedral sites (96h). The Ca^{2+} ions were located in dodecahedral sites. The Er^{3+} ions replace for the Ca^{2+} ones in these sites, their corresponding occupancy rate converged well with the Rietveld calculation. The interatomic distances Ca | Er—O were calculated and collected in the Table 3. The 16a positions are fully occupied by Nb^{5+} and Ga^{3+} in a ratio of about ≈2:1. The corresponding Nb1 | Ga1—O bond lengths is 1.970(2) Å for 10 at.% Er^{3+} then it increased to 2.133(0) Å for 30 at.% Er^{3+}. While, the 24d sites were occupied by the other fraction of Ga^{3+} (predominantly) and Nb^{5+} (a very small amount), Li^+ incorporation was this garnet host takes place only at 24d site (≈10%), as previously reported from similar structure study with powder neutron diffraction (pND) [28]. The random distribution of the Ga^{3+} and Nb^{5+} cations over the octahedral and tetrahedral sites determines the disordered crystal structure. The

shortest intermetallic distances Ca | Er–Ca | Er 3.825(1) Å 10 at.% Er^{3+} then it decreased slightly to 3.811(5) Å for 30 at.% Er^{3+}.

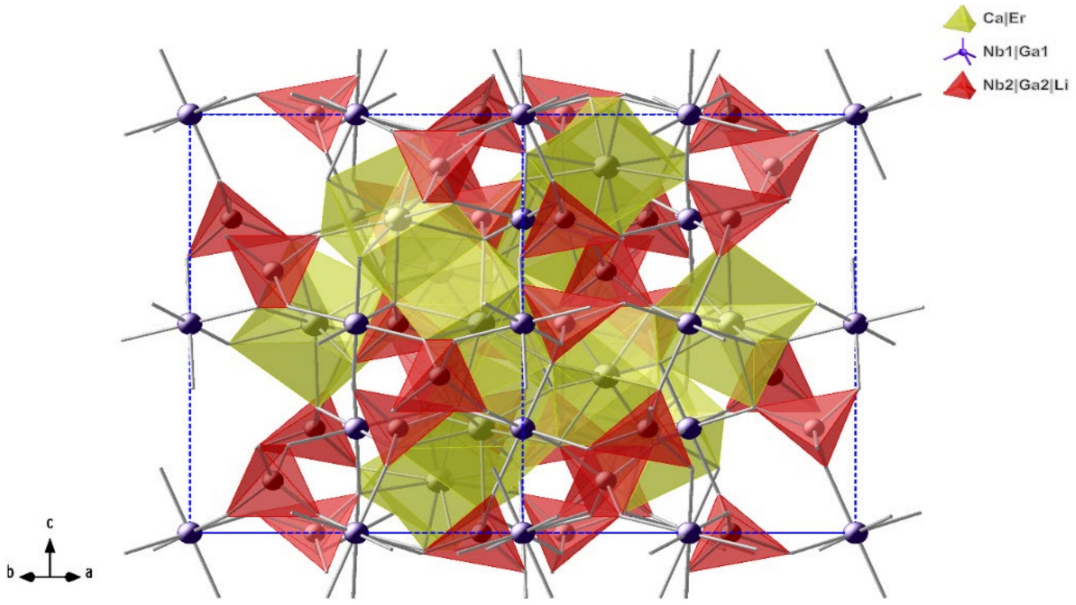

Figure 4. Unit-cell representation of Er:CLNGG crystal in the (110) crystallographic plan.

Table 3. Bond lengths and intermetallic distances (Å) in 10, 15 and 30 at % Er:CLNGG crystals.

Distances(Å)	10 at.% Er:CLNGG	15 at.% Er:CLNGG	30 at.% Er:CLNGG
Ca | Er—O	1.831(1) × 4	1.778(1) × 4	1.728(7) × 4
	3.641(4) × 4	3.731(7) × 4	3.660(3) × 4
Nb1 | Ga1—O	1.970(2) × 6	2.018(8) × 6	2.133(0) × 6
Nb2 | Ga2 | Li—O	2.295(5) × 4	2.390(3) × 4	2.464(1) × 4
Ca | Er—Ca | Er	3.825(1) × 4	3.820(1) × 4	3.811(5) × 4
	5.843(0) × 4	5.820(3) × 4	5.822(2) × 4
Ca | Er—Nb1 | Ga1	3.491(8) × 4	3.487(3) × 4	3.479(4) × 4
Ca | Er—Nb1 | Ga1 | Li	3.123(2) × 2	3.119(1) × 2	3.112(1) × 2
	3.491(8) × 4	3.487(3) × 4	3.479(4) × 2

3.2. Thermal Properties

3.2.1. Specific Heat

Figure 5 shows the relationship between the temperature and specific heat of Er:CLNGG. It could be found that the specific heat varies almost linearly, increasing with the increasing temperature. At 298.15 K, the specific heat of 10 at.% Er:CLNGG was 0.64 J g^{-1} K^{-1}, 15 at.% Er:CLNGG and 30 at.% Er:CLNGG was 0.77 J g^{-1} K^{-1} and 0.60 J g^{-1} K^{-1} respectively. The specific heat of Er:CLNGG was slightly larger in contrast to Nd:YAG (0.59 J g^{-1} K^{-1}) and Nd:YVO_4 (0.51 J g^{-1} K^{-1}) [29,30], indicating that the Er:CLNGG should have high damage threshold.

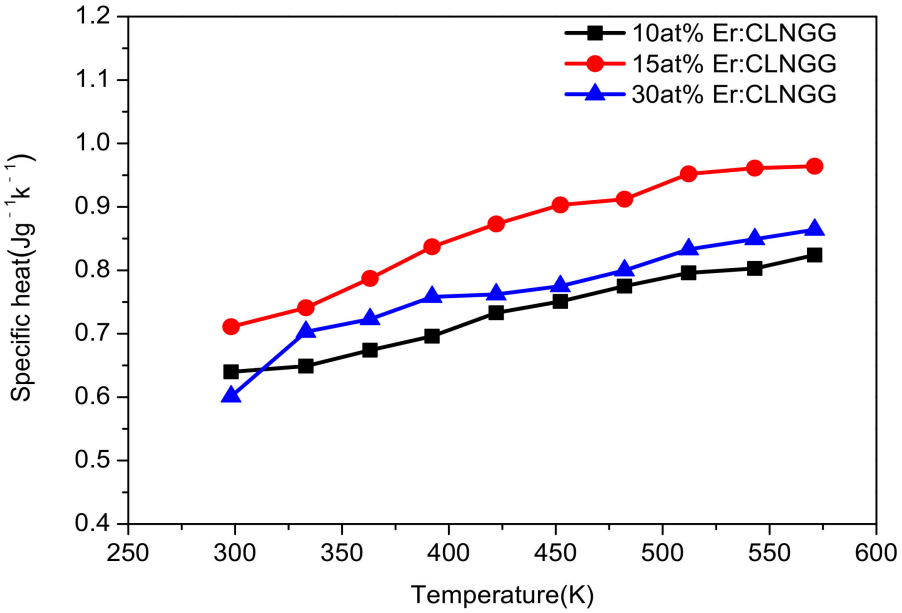

Figure 5. Specific heat of Er:CLNGG crystal as a function of temperature.

3.2.2. Thermal Diffusion Coefficient

The thermal diffusion coefficient, which is symmetric second-rank tensor, is a physical quantity to explain the ability of the heat to diffuse inside the crystal. The dependence of thermal diffusion coefficient of crystal on temperature was shown in the Figure 6. It could be seen that the thermal diffusion coefficient of Er:CLNGG crystal decrease with increasing temperature. At 298.15 K, the thermal diffusion coefficient is 1.027 mm^2/s for 10 at.% Er:CLNGG, 0.997 mm^2/s for 15 at.% Er:CLNGG and 0.821 mm^2/s for 30 at.% Er:CLNGG, respectively.

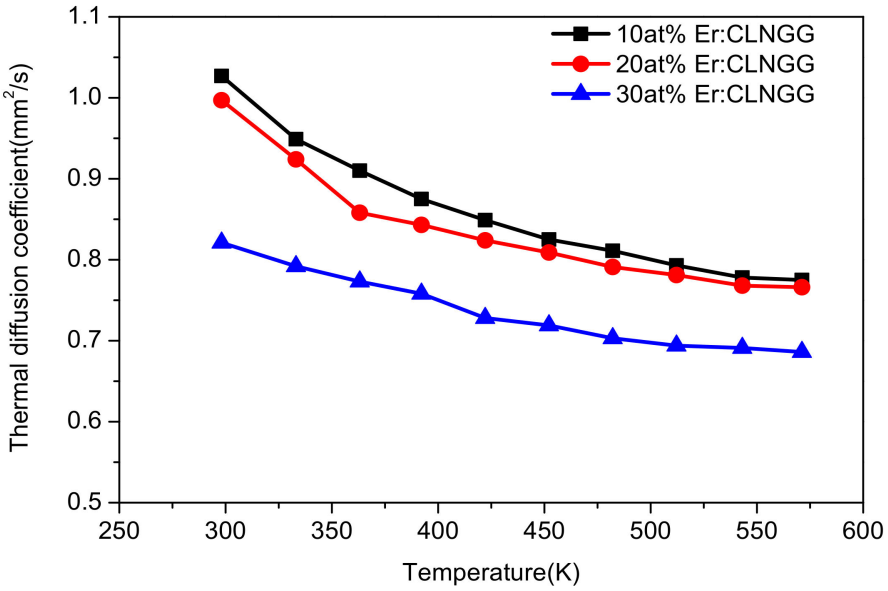

Figure 6. Thermal diffusion coefficient of Er:CLNGG crystal as a function of temperature.

3.2.3. Thermal Conductivity

The thermal conductivity of Er:CLNGG versus the temperature in 298.15–571.15 K was shown in Figure 7. The thermal conductivity was determined by using the followed equation:

$$k = \lambda \times \rho \times C_p \quad (4)$$

where the λ is thermal diffusivity coefficient, ρ is the density of crystal and C_p is the specific heat. It can be seen that the thermal conductivity of Er:CLNGG increases with increasing temperature, indicating a typical glass-like behavior, which is possibly related to the disordered structure of the crystal [24]. At room temperature (RT, 300 K), the thermal conductivities are 3.26, 3.68, and 3.01 W m^{-1} K^{-1} for the 10 at.% Er:CLNGG, 15 at.% Er:CLNGG, and 30 at.% Er:CLNGG crystals, respectively.

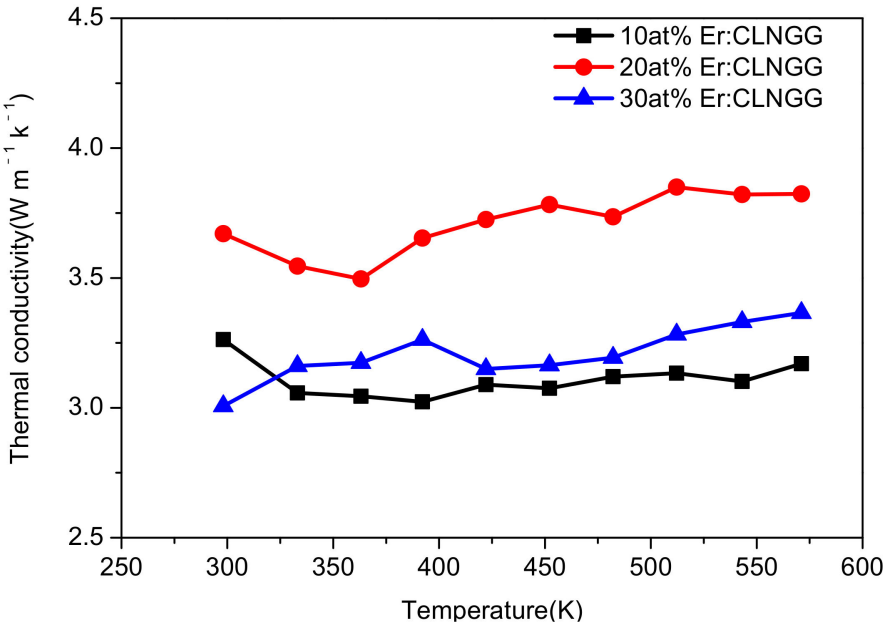

Figure 7. Thermal conductivity of Er:CLNGG crystal as a function of temperature.

3.3. Spectroscopic Characteristics

3.3.1. Absorption Spectra

Figure 8 presents the room temperature absorption spectra of Er^{3+} doped CLNGG crystals with different erbium concentration. Several typical absorption bands of Er:CLNGG can be obviously observed, corresponding to the transition of Er^{3+} ion from $^4I_{15/2}$ ground state to the excited states. For clear comparisons, the enlarged 970 nm absorption bands of Er^{3+} ions with different concentration were shown in the inset of Figure 8. In can be seen that the full widths at half-maximum (FWHM) at ~970 nm of these samples were similar, which were about 40 nm, much wider than other ordered garnet crystal, such as Er:LuSGG (FWHM = 11 nm) [31]. This phenomenon is beneficial to reduce the temperature dependence of laser diode and improve the laser efficiency. The absorption cross-section can be calculated by the following equation:

$$\sigma_{abs} = \frac{\alpha(\lambda)}{N_0} \quad (5)$$

In this equation, where $\alpha(\lambda)$ is absorption coefficient, N_0 is concentration of Er^{3+} ions in the CLNGG. Then the absorption cross-section with peak at ~970 nm are calculated to be 1.93×10^{-21} cm^2 for 10 at.% Er:CLNGG, 2.07×10^{-21} cm^2 for 15 at.% Er:CLNGG, 0.87×10^{-21} cm^2 for 30 at.% Er:CLNGG, respectively.

The standard Judd-Ofelt (J-O) theory was applied to analyze the absorption spectra. More details for the case of Er^{3+}-doped crystals can be found elsewhere [32]. Here the intensity (J-O) parameters are as follows: $\Omega_2 = 2.44$, $\Omega_4 = 2.23$ and $\Omega_6 = 0.44$ [10^{-20} cm^2] for 10 at.% Er:CLNGG, $\Omega_2 = 2.92$, $\Omega_4 = 3.60$ and $\Omega_6 = 1.02$ [10^{-20} cm^2] for 20 at.% Er:CLNGG and $\Omega_2 = 1.57$, $\Omega_4 = 1.97$, and $\Omega_6 = 0.33$ [10^{-20} cm^2] for 30 at.% Er:CLNGG, respectively. On the basis of the J-O modelling, the radiative lifetimes of the excited states τ_{rad} can be

calculated. The radiative lifetime τ_{rad} of the $^4I_{11/2}$ upper laser level was calculated to be 3.89, 3.41, and 8.55 ms for the mentioned Er:CLNGG crystals, respectively.

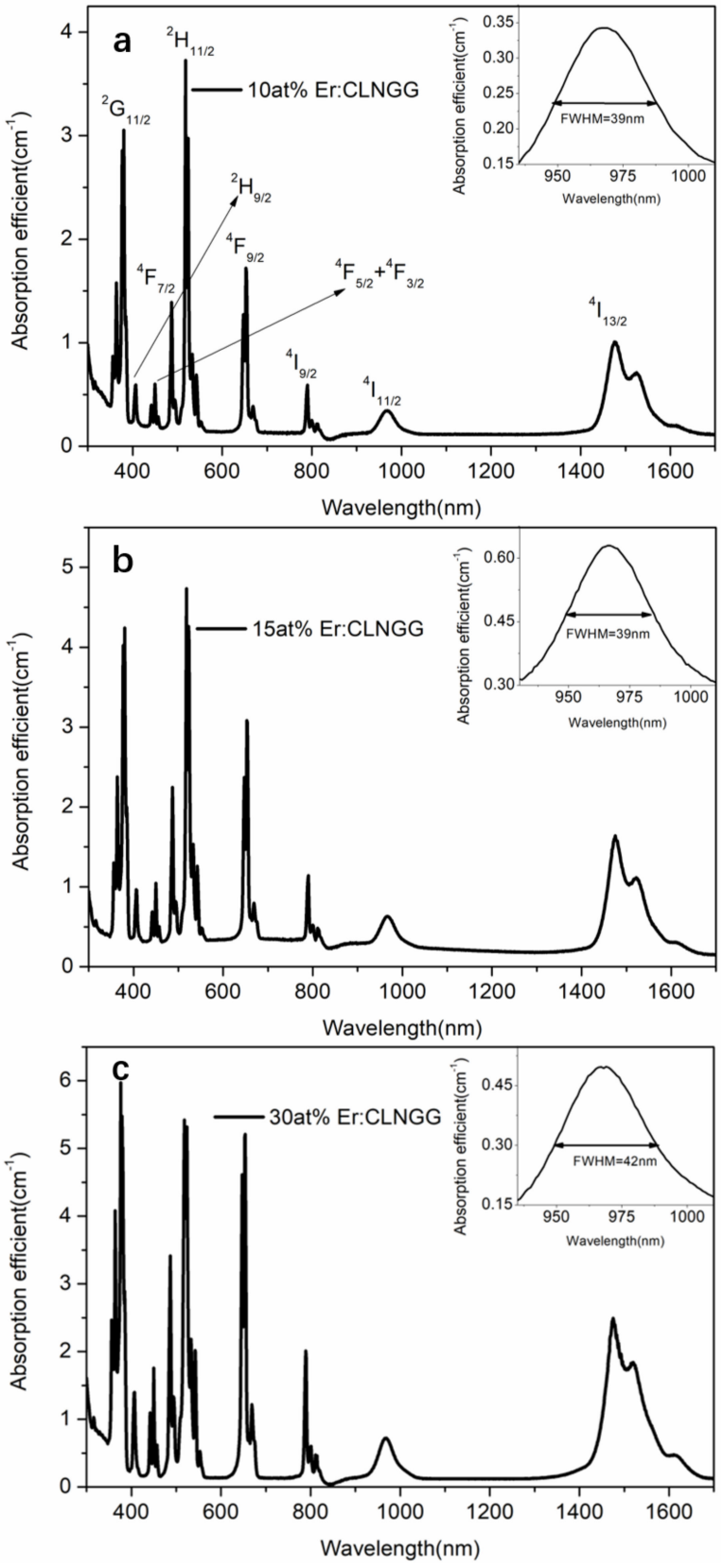

Figure 8. Absorption spectrum of (**a**) 10 at.% Er: CLNGG (**b**) 15 at.% Er: CLNGG (**c**) 30 at.% Er:CLNGG from 350 nm to 1650 nm.

3.3.2. Emission Spectra

The near-infrared (NIR) fluorescence spectra (Figure 9a) of Er:CLNGG in the region of 1400–1800 nm were measured under excitation at 987 nm. Results show that the intense fluorescence bands are centered at around 1630 nm, corresponding to the transition of Er^{3+}:$^4I_{13/2}\rightarrow{}^4I_{15/2}$. With the increasing of Er^{3+} ions concentration, the intensity of the fluorescence bands around 1630 nm become weaker and weaker.

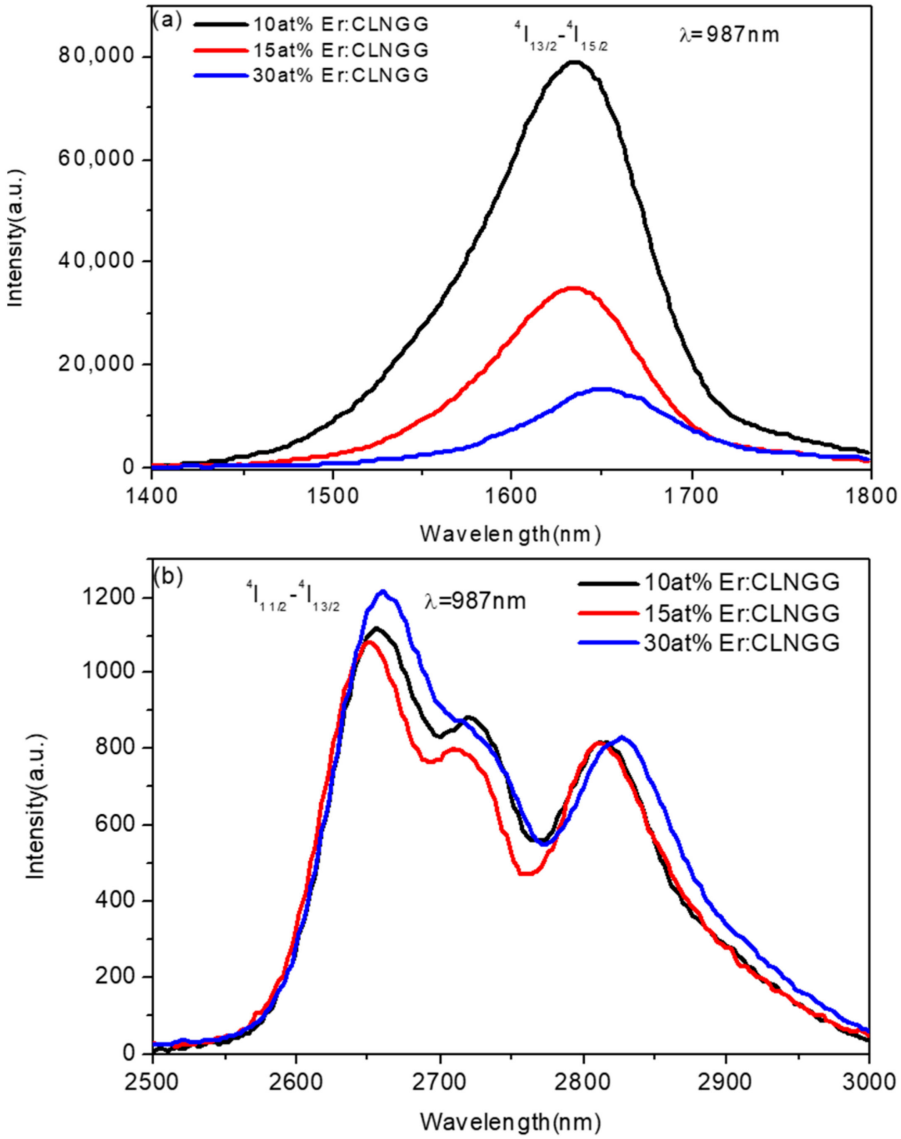

Figure 9. Emission spectra of Er:CLNGG ranging from (**a**) 1400–1800 nm (**b**) 2500–3000 nm under the excitation of 987 nm.

The mid-infrared emission (MIR) spectra of Er:CLNGG in the region of 2500–3000 nm are shown in Figure 9b, which were excited by an optical parametric oscillator (OPO) laser at 987 nm. The strongest emission band are centered at around 2650 nm, corresponding to the Er^{3+}:$^4I_{11/2}\rightarrow{}^4I_{13/2}$ transition. It can also be seen that the emission band around 2700 nm were very broad, ranging from 2500 to 3000 nm, which is very suitable for the ultra-short pulse laser generation. In addition, with the Er^{3+} ions concentration increases to 30 at.%, the emission intensity shows a relatively obvious enhancement.

According to the emission spectra, the RT stimulated-emission (SE) cross-sections, σ_{SE}, for the $^4I_{11/2} \rightarrow {}^4I^{13/2}$ transition of Er^{3+} ions were calculated by the Füchtbauer-Ladenburg (F-L) formula and illustrated in Figure 10.

$$\sigma_{SE} = \frac{1}{8\pi n^2 c \tau_{rad}} \frac{\lambda^5 I(\lambda)}{\int \lambda I(\lambda) d\lambda} \quad (6)$$

where λ is the wavelength, τ_{rad} is the radiative lifetimes of the excited states, $I(\lambda)$ is the emission spectrum, c is the light speed, and n is the refractive index. It could be seen that the maximum emission cross-sections of Er:CLNGG with different Er^{3+} concentration are estimated to be 2.11×10^{-20}, 1.29×10^{-20}, and 0.98×10^{-20} cm^2 at around 2650 nm, respectively. Besides, the obtained spectral parameters of Er:CLNGG as well as the other several crystals are also listed in Table 4.

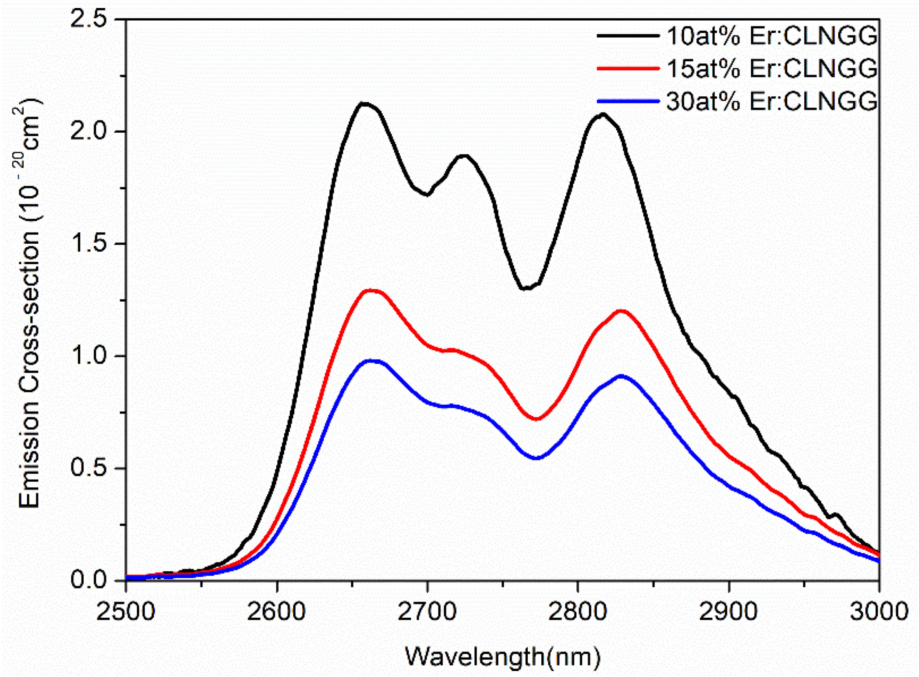

Figure 10. Emission cross-sections for the $^4I_{11/2} \rightarrow {}^4I_{13/2}$ transition.

Table 4. Spectral parameters of several erbium doped crystals.

Crystal	σ_{abs} (20^{-21} cm^2)	σ_{ES} (20^{-19} cm^2)	$^4I_{11/2}$ Lifetime (ms)	$^4I_{13/2}$ Lifetime (ms)	$^4I_{11/2}$ (%) Quantum Efficiency	Ref.
Er:YSGG	1.56@790 nm	1.02@2640 nm	0.57	2.06	-	[33,34]
Er:$CaLaGa_3O_7$	1.91@969 nm	1.79@2702 nm	0.77	8.41	19.8	[32]
50at%Er:YAG	-	0.3@2936 nm	0.12	7.25	-	[35,36]
20 at.%Er:LuGG	4.33@967 nm	0.43@2705 nm	0.7	10	-	[7]
10at%Er:CLNGG	1.93@968 nm	0.21@2664 nm	0.57	4.06	14.0	This work
15at%Er:CLNGG	2.07@966 nm	0.13@2660 nm	0.56	3.56	15.7	
30at%Er:CLNGG	0.87@970 nm	0.08@2664 nm	0.45	1.58	28.5	

3.3.3. Fluorescence Lifetime

For the laser crystal, the fluorescence lifetime is a significant parameter to judge the 3-μm laser performance. Here, the fluorescence decay curves measured upon direct excitation of $^4I_{11/2}$ are shown in Figure 11. It can be found that the fluorescence lifetimes of

Er:CLNGG crystal are well fitted to the exponential decaying behavior, which would be defined by the following formula:

$$I(t) = A + Be^{-\frac{t}{\tau}} \quad (7)$$

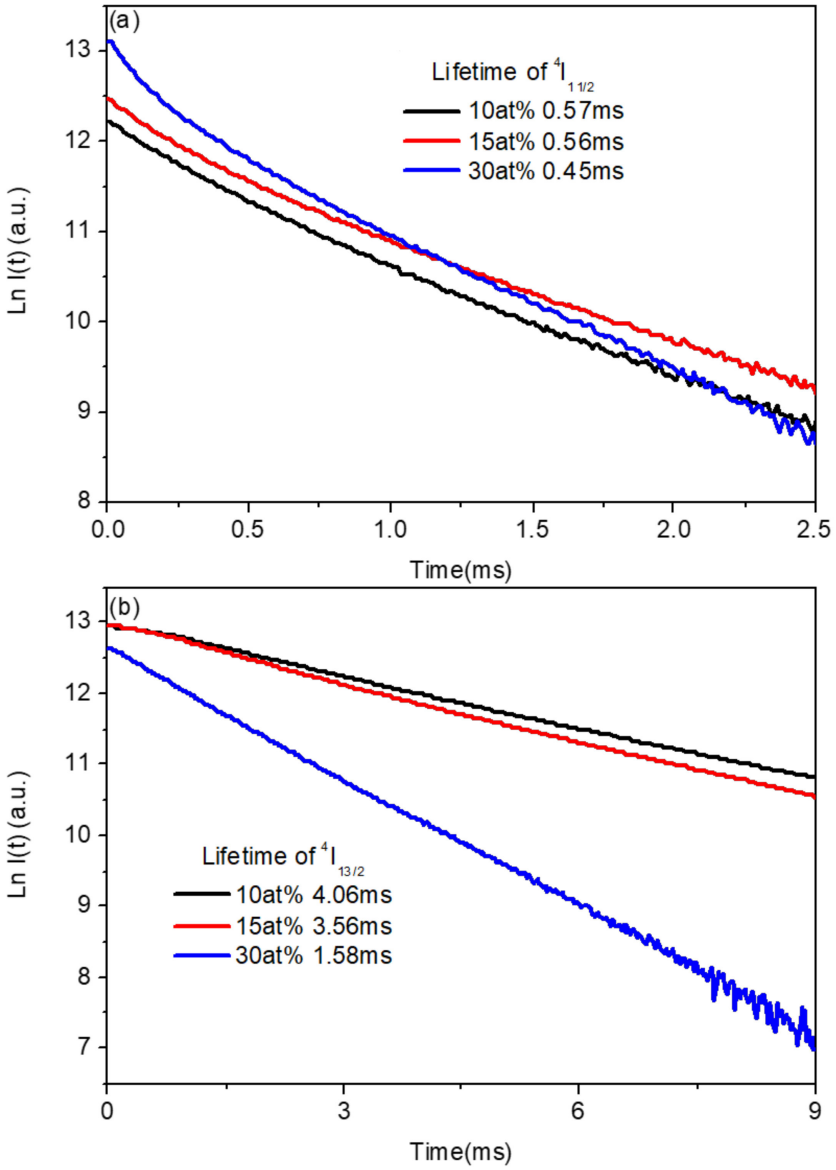

Figure 11. Fluorescence decay time of (**a**) $^4I_{11/2}$ and (**b**) $^4I_{13/2}$ with different concentration of Er^{3+} ions at room temperature.

As shown in the Figure 11a,b, the fluorescence lifetimes of Er:$^4I_{13/2}$ and $^4I_{11/2}$ levels in CLNGG are all decreased with incensement of Er^{3+} ions concentration. What is noteworthy is that the lifetime of $^4I_{13/2}$ decreased much faster than that of lifetime of $^4I_{11/2}$ when the concentration of Er^{3+} ions increases from 10 at.% to 30 at.%. This phenomenon is beneficial to surmount the "bottleneck" effect. The difference of lifetime between $^4I_{13/2}$ and $^4I_{11/2}$ is decreased from 3.5 ms (10 at.% Er:CLNGG) to 1.13 ms (30 at.% Er:CLNGG). Taking into account the trends of the fluorescence lifetimes, we can infer that the 30 at.% Er:CLNGG crystal is a more suitable candidate for 3-μm laser.

4. Conclusions

To conclude, a series of Er:CLNGG crystals with different Er^{3+} ion concentrations (10, 15 and 30 at.%) was successfully grown by the Cz method. Its structure and thermal performance were investigated. Structure results reveal that the random distribution of the Ga^{3+} and Nb^{5+} cations over the octahedral and tetrahedral sites determines the disordered crystal structure. The thermal conductivities of Er:CLNGG (10 at.%, 15 at.%, and 30 at.%) at RT are 3.26, 3.68, and 3.01 W m^{-1} K^{-1}, respectively. Additionally, properties of absorption, emission and fluorescence lifetime were also investigated. Three highest absorption cross-section at 978 nm were obtained for the 10 at.%, 15 at.%, and 30 at.% Er:CLNGG crystals with the value of 1.93 × 10^{-21} cm^2, 2.07 × 10^{-21} cm^2 and 0.87 × 10^{-21} cm^2, respectively. Effect of Er^{3+} concentration on emission and fluorescence lifetime of Er:CLNGG crystals was studied. Results show that with the Er^{3+} concentration increase, the emission of the Er^{3+}:$^4I_{13/2}$→$^4I_{15/2}$ transitions weakened, while the Er^{3+}:$^4I_{11/2}$→$^4I_{13/2}$ strengthened. Fluorescence lifetime of $^4I_{13/2}$ decreased faster than that of $^4I_{11/2}$ with the Er^{3+} concentration increase, which is beneficial for overcoming the "bottleneck" effect to achieve 2.7 μm laser. All the results suggest that Er:CLNGG crystal can be a potential candidate for the 2.7 μm laser, especially with the high Er^{3+} ions concentration.

Author Contributions: Conceptualization, K.T. and Z.P.; methodology, K.T. and Z.P.; investigation, K.T.; resources, S.Y. and J.G.; writing—original draft preparation, K.T.; writing—review and editing, Z.P. and J.G. All authors have read and agreed to the published version of the manuscript.

Funding: This research was funded by National Natural Science Foundation of China (projects No. 52072351), Foundation of the President of China Academy of Engineering Physics (project No. YZJJLX2018005), Fund of Key Laboratory of Optoelectronic Materials Chemistry and Physics, Chinese Academy of Sciences (project No. 2008DP173016).

Institutional Review Board Statement: Not applicable.

Informed Consent Statement: Not applicable.

Data Availability Statement: Data is contained within the article.

Acknowledgments: The authors thank Xavier Mateos and Sami Slimi (Universitat Rovira i Virgili, Spain) for the help on the structure analysis.

Conflicts of Interest: The authors declare no conflict of interest.

References

1. Xu, R.R.; Tian, Y.; Hu, L.L.; Zhang, J.J. Enhanced emission of 2.7 μm pumped by laser diode from Er^{3+}/Pr^{3+}-codoped germanate glasses. *Opt. Lett.* **2011**, *36*, 1173–1175. [CrossRef] [PubMed]
2. Zajac, A.; Skorczakowski, M.; Swiderski, J.; Nyga, P. Electrooptically Q-switched mid-infrared Er:YAG laser for medical applications. *Opt. Express* **2004**, *12*, 5125–5130. [CrossRef] [PubMed]
3. Vodopyanov, K.L. Mid-infrared optical parametric generator with extra-wide (3–19 μm) tunability: Applications for spectroscopy of two-dimensional electrons in quantum wells. *J. Opt. Soc. Am. B* **1999**, *16*, 1579–1586. [CrossRef]
4. Vodopyanov, K.L.; Ganikhanov, F.; Maffetone, J.P.; Zwieback, I.; Ruderman, W. $ZnGeP_2$ optical parametric oscillator with 3.8–12.4 μm tenability. *Opt. Lett.* **2000**, *25*, 841–843. [CrossRef] [PubMed]
5. Ziolek, C.; Ernst, H.; Will, G.F.; Lubatschowski, H.; Welling, H.; Ertmer, W. High-repetition-rate, high average-power, diode-pumped 2.94-microm Er:YAG laser. *Opt. Lett.* **2001**, *26*, 599–601. [CrossRef] [PubMed]
6. You, Z.Y.; Wang, Y.; Xu, J.L.; Zhu, Z.J.; Li, J.F.; Wang, H.Y.; Tu, C.Y. Single-longitudinal-mode Er:GGG microchip laser operating at 2.7 μm. *Opt. Lett.* **2015**, *40*, 3846–3849. [CrossRef] [PubMed]
7. You, Z.Y.; Li, J.F.; Wang, Y.; Chen, H.B.; Zhu, Z.J.; Tu, C.Y. Spectroscopic and laser properties of Er:LuGG crystal at 2.8 μm. *Appl. Phys. Express* **2019**, *12*, 052019. [CrossRef]
8. You, L.; Lu, D.Z.; Pan, Z.B.; Yu, H.H.; Zhang, H.J.; Wang, J.Y. High-efficiency 3 μm Er:YGG crystal lasers. *Opt. Lett.* **2018**, *43*, 5873–5876. [CrossRef]
9. Nie, H.K.; Hu, Q.Q.; Zhang, B.T.; Sun, X.L.; Tian, H.L.; Wang, Y.R.; Yan, B.Z.; Jia, Z.T.; Yang, K.J.; Tao, X.T.; et al. Highly Efficient Continuous-Wave and Passively Q-Switching 2.8-μm Er:YSGG Laser. *IEEE Photonics Technol. Lett.* **2018**, *30*, 1400–1403. [CrossRef]
10. Zhao, X.Y.; Sun, D.L.; Luo, J.Q.; Zhang, H.L.; Fang, Z.Q.; Quan, C.; Hu, L.Z.; Cheng, M.J.; Zhang, Q.L.; Yin, S.T. Laser performance of a 966 nm LD side-pumped Er,Pr:GYSGG laser crystal operated at 2.79 μm. *Opt. Lett.* **2018**, *43*, 4312–4315. [CrossRef]

11. Wang, J.T.; Cheng, T.Q.; Wang, L.; Yang, J.W.; Sun, D.L.; Yin, S.T.; Wu, X.Y.; Jiang, H. Compensation of strong thermal lensing in an LD side-pumped high-power Er: YSGG laser. *Laser Phys. Lett.* **2015**, *12*, 105004. [CrossRef]
12. Hu, Q.Q.; Nie, H.K.; Mu, W.X.; Yin, Y.R.; Zhang, J.; Zhang, B.T.; He, J.L.; Jia, Z.T.; Tao, X.T. Bulk growth and an efficient mid-IR laser of high-quality Er:YSGG crystals. *CrystEngComm* **2019**, *21*, 1928–1933. [CrossRef]
13. Gao, J.Y.; Sun, D.L.; Zhang, Q.L.; Wang, X.F.; Liu, W.P.; Luo, J.Q.; Sun, G.H.; Yin, S.T. Experimental investigation and crystal-field modeling of Er^{3+} energy levels in GSGG crystal. *J. Alloys Compd.* **2016**, *671*, 389–395. [CrossRef]
14. Sun, D.L.; Luo, J.Q.; Xiao, J.Z.; Zhang, Q.L.; Chen, J.K.; Liu, W.P.; Kang, H.X.; Yin, S.T. Luminescence and thermal properties of Er: GSGG and Yb,Er: GSGG laser crystals. *Chin. Phys. Lett.* **2012**, *29*, 054209. [CrossRef]
15. Zhang, Y.S.; Cai, Y.; Xu, B.; Zhang, J.; Zhao, L.; Liu, P.; Xu, X.D. Single-mode oscillations of diode-pumped mid-infrared Er:Y_2O_3 ceramic microchip lasers at 2.7 μm. *Opt. Express* **2019**, *27*, 31783–31789. [CrossRef]
16. Sanamyan, T.; Kanskar, M.; Xiao, Y.; Kedlaya, D.; Dubinskii, M.M. High power diode-pumped 2.7 μm Er^{3+}: Y_2O_3 laser with nearly quantum defect-limited efficiency. *Opt. Express* **2011**, *19*, A1082–A1087. [CrossRef]
17. Uehara, H.; Tokita, S.; Kawanaka, J.; Konishi, D.; Murakami, M.; Yasuhara, R. A passively Q-switched compact Er: Lu_2O_3 ceramics laser at 2.8 μm with a graphene saturable absorber. *Appl. Phys. Express* **2019**, *12*, 022002. [CrossRef]
18. Labbe, C.; Doualan, J.L.; Camy, P.; Moncorge, R.; Thuau, M. The 2.8 μm laser properties of Er^{3+} doped CaF_2 crystals. *Opt. Commun.* **2002**, *209*, 193–199. [CrossRef]
19. Šulc, J.; Němec, M.; Svejkar, R.; Jelínková, H.; Doroshenko, M.E.; Fedorov, P.P.; Osiko, V.V. Diodepumped Er: CaF_2 ceramic 2.7 μm tunable laser. *Opt. Lett* **2013**, *38*, 3406–3409. [CrossRef]
20. Fan, M.Q.; Li, T.; Zhao, J.; Zhao, S.Z.; Li, G.Q.; Yang, K.J.; Su, L.B.; Ma, H.Y.; Kränkel, C. Continuous wave and ReS_2 passively Q-switched Er: SrF_2 laser at ~3 μm. *Opt. Lett.* **2018**, *43*, 1726–1729. [CrossRef]
21. Gorbachenya, K.N.; Kurilchik, S.V.; Kisel, V.E.; Yasukevich, A.S.; Kuleshov, N.V.; Nizamutdinov, A.S.; Korableva, S.L.; Semashko, V.V. Laser performance of inband pumped Er: $LiYF_4$ and Er: $LiLuF_4$ crystals. *Quantum Electron.* **2016**, *46*, 95–99. [CrossRef]
22. Tang, P.H.; Wu, M.; Wang, Q.K.; Miao, L.L.; Huang, B.; Liu, J.; Zhao, C.J.; Wen, S.C. 2.8 mm pulsed Er^{3+}: ZBLAN fiber laser modulated by topological insulator. *IEEE Photonics Technol. Lett.* **2016**, *28*, 1573–1576. [CrossRef]
23. Wang, Y.; Li, J.F.; Zhu, Z.J.; Xu, J.L.; Tu, C.Y. Crystal growth and optical properties of Cr^{3+}, Er^{3+}, RE^{3+}:$Gd_3Ga_5O_{12}$ (RE = Tm, Ho, Eu) for mid-IR laser applications. *J. Lumin.* **2012**, *132*, 693–696. [CrossRef]
24. Pan, Z.B.; Loiko, P.; Wang, Y.C.; Zhao, Y.G.; Yuan, H.L.; Tang, K.Y.; Dai, X.J.; Cai, H.Q.; Serres, J.M.; Slimi, S.; et al. Disordered Tm^{3+},Ho^{3+}-codoped CNGG garnet crystal: Towards efficient laser materials for ultrashort pulse generation at ~2 μm. *J. Alloys Compd.* **2021**, *853*, 157100. [CrossRef]
25. Li, K.Y.; Xue, D.F. A new set of electronegativity scale for trivalent lanthanides. *Phys. Status Solidi B* **2007**, *244*, 1982–1987. [CrossRef]
26. Novak, G.A.; Gibbs, G.V. The crystal chemistry of the silicate garnets. *Am. Miner.* **1971**, *56*, 791–825.
27. Yuiga, N.; Shibayama, N.; Hori, A.; Matsushita, T.; Segawa, H.; Kondo, T. Crystal Systems and Lattice Parameters of $CH_3NH_3Pb(I_{1-x}Br_x)_3$ Determined Using Single Crystals: Validity of Vegard's Law. *Inorg. Chem.* **2020**, *59*, 6709–6716.
28. Jumpei, U.; Tanabe, S. Review of Luminescent Properties of Ce^{3+}-Doped Garnet Phosphors: New Insight into the Effect of Crystal and Electronic Structure. *Opt. Mater.* **2019**, *1*, 100018.
29. Pan, Z.B.; Cong, H.J.; Yu, H.H.; Tian, L.; Yuan, H.; Cai, H.Q.; Zhang, H.J.; Huang, H.; Wang, J.Y.; Wang, Q.; et al. Growth, thermal properties and laser operation of Nd:$Ca_3La_2(BO_3)_4$: A new disordered laser crystal. *Opt. Express* **2013**, *21*, 6091–6100. [CrossRef]
30. Zhang, H.J.; Zhu, L.; Meng, X.L.; Yang, Z.H.; Wang, C.Q.; Yu, W.T.; Chow, Y.T.; Lu, M.K. Thermal and Laser Properties of Nd:YVO_4 Crystal. *Cryst. Res. Technol.* **1999**, *34*, 1011–1016. [CrossRef]
31. Zhao, X.Y.; Sun, D.L.; Luo, J.Q.; Zhang, H.L.; Quan, C.; Hu, L.Z.; Han, Z.Y.; Dong, K.P.; Cheng, M.J.; Yin, S.T. Spectroscopic and laser properties of Er:LuSGG crystal for high-power ~2.8 μm mid-infrared laser. *Opt. Express* **2020**, *28*, 8843–8852. [CrossRef] [PubMed]
32. Liu, Y.Y.; Wang, Y.; You, Z.Y.; Li, J.F.; Zhu, Z.J.; Tu, C.Y. Growth, structure and spectroscopic properties of melilite Er: CaLaGa3O7 crystal for use in mid-infrared laser. *J. Alloys Compd.* **2017**, *706*, 387–394. [CrossRef]
33. Wang, Y.; Li, J.F.; Zhu, Z.J.; You, Z.Y.; Xu, J.L.; Tu, C.Y. Bulk Crystal Growth, First-Principles Calculation, and Optical Properties of Pure and Er^{3+} Doped $SrLaGa_3O_7$ Single Crystals. *Cryst. Growth Des.* **2016**, *6*, 2289–2294. [CrossRef]
34. Sardar, D.K.; Bradley, W.M.; Perez, J.J. Judd–Ofelt analysis of the Er^{3+} ($4f^{11}$) absorption intensities in Er^{3+}–doped garnets. *J. Appl. Phys.* **2003**, *93*, 2602–2607. [CrossRef]
35. Dinerman, B.J.; Moulton, P.F. 3-μm cw laser operations in erbium-doped YSGG, GGG, and YAG. *Opt. Lett.* **1994**, *19*, 1143–1145. [CrossRef]
36. Arbabzadah, E.; Chard, S.; Amrania, H.; Phillips, C.; Damzen, M. Comparison of a diode pumped Er:YSGG and Er:YAG laser in the bounce geometry at the 3 μm transition. *Opt. Express* **2011**, *19*, 25860–25865. [CrossRef]